

# Modelling leaky photonic wires: A mode solver comparison

P. BIENSTMAN<sup>1,\*</sup>, S. SELLERI<sup>2</sup>, L. ROSA<sup>2</sup>, H.P. URANUS<sup>3</sup>,  
W.C.L. HOPMAN<sup>3</sup>, R. COSTA<sup>4</sup>, A. MELLONI<sup>5</sup>,  
L.C. ANDREANI<sup>6</sup>, J.P. HUGONIN<sup>7</sup>, P. LALANNE<sup>7</sup>,  
D. PINTO<sup>8</sup>, S.S.A. OBAYYA<sup>8</sup>, M. DEMS<sup>9</sup>, AND  
K. PANAJOTOV<sup>10</sup>

<sup>1</sup>*Ghent University, Sint-Pietersnieuwstraat 41, Ghent 9000, Belgium*

(\*author for correspondence: E-mail: Peter.Bienstman@UGent.be)

<sup>2</sup>*Università degli Studi di Parma, Parco Area delle Scienze 181/A, I-43100Parma,Italy*

<sup>3</sup>*University of Twente, P.O. Box 217, 7500 AE, Enschede, The Netherlands*

<sup>4</sup>*CoreCom, Via G. Colombo 34/5, Milano, Italy*

<sup>5</sup>*Dipartimento di Elettronica e Informazione, Politecnico di Milano, Via Ponzio 34/5, Milano, Italy*

<sup>6</sup>*Dipartimento di Fisica "A. Volta", Università degli Studi di Pavia, Via Bassi 6, Pavia, I-27100 Italy*

<sup>7</sup>*Laboratoire Charles Fabry de l'Institut d'Optique, CNRS, Univ Paris-Sud, Campus Polytechnique, RD128, 91127 Palaiseau cedex, France*

<sup>8</sup>*Institute of Advanced Telecommunications, University of Wales Swansea, Singleton Park, Swansea, SA2 8PP, UK*

<sup>9</sup>*Institute of Physics, Technical University of Lodz, ul. Wolczanska 219, Lodz, 93–005 Poland*

<sup>10</sup>*Department of Applied Physics and Photonics, Vrije Universiteit Brussel, Pleinlaan 2, Brussels, 1050 Belgium*

Received: 25 July 2006; accepted: 3 November 2006

**Abstract.** We present results from a mode solver comparison held within the framework of the European COST P11 project. The structure modelled is a high-index contrast photonic wire in silicon-on-insulator subject to substrate leakage. The methods compared are both in-house developed and commercial, and range from effective index and perturbation methods, over finite-element and finite-difference codes, beam propagation methods, to film mode matching methods and plane wave expansion methods.

**Key words:** optical mode solvers, photonic wires, substrate leakage, waveguides

## 1. Introduction

During the past, there has been a tradition of comparing the current state-of-the-art optical mode solvers from time to time (Vassallo 1997; Selleri and Petracek 2001; Selleri *et al.* 2001; Ctyroky *et al.* 2002). In the framework of the European COST P11 action (COST P11), we performed such a comparison, but this time with an additional complication, namely the modelling of an extremely small loss in the propagation constant due to substrate leakage.

The structure we modeled is the following photonic wire structure in the SOI material system (Dumon *et al.* 2004), as shown in Fig. 1. It consists

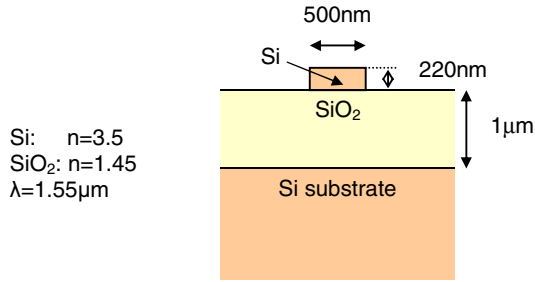


Fig. 1. Photonic wire structure modeled.

of a 500 nm wide waveguide in a Si layer of 220 nm thick, sitting on top of a 1  $\mu\text{m}$  thick SiO<sub>2</sub> buffer, which in turn is sitting on a Si substrate. The wavelength considered is 1.55  $\mu\text{m}$  and the refractive indices of Si and SiO<sub>2</sub> are 3.5 and 1.45, respectively. The top cladding is air with index 1.

Because of the limited thickness of the oxide buffer, some part of the power in the fundamental mode will leak to the substrate. The aim of this comparison is to calculate the complex propagation constant of the fundamental mode of this structure as accurately as possible.

The rest of this paper is structured as follows: first, a brief description of each method and the results obtained with it is given. Then, all the results are brought together in a table and discussed.

The methods that are being compared are:

- An effective index method (R. Costa, A. Melloni)
- A perturbative approach (L.C. Andreani)
- BPM code (D. Pinto, S. Obayya)
- A finite element code by H. Uranus
- A finite element code by S. Selleri and L. Rosa
- Olympios, a commercial finite difference solver (W. Hopman)
- Fimmwave, a commercial film mode matching solver (R. Costa, A. Melloni)
- A film mode matching solver by P. Bienstman
- A plane wave code by P. Lalanne and J.P. Hugonin
- A plane wave admittance code by M. Dems

We also want to point out that the results with commercial tools were obtained by users, not by their developers, which leaves open the possibility that more accurate results could be obtained by the developers of the code.

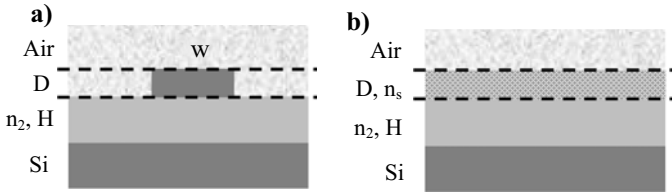


Fig. 2. The effective index approach reduces the original problem (a) to an equivalent slab (b).

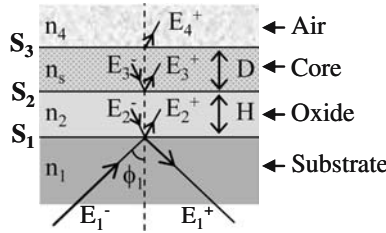


Fig. 3. E-field components in the leaky slab in case of incidence of a plane wave from the substrate.

### 2. Effective index method

A simple approximate method to calculate the complex propagation constant of the considered optical waveguide is based on the solution of an equivalent leaky slab waveguide by the transfer matrix method (TMM) (Ghatak *et al.* 1987). The 2D waveguide problem (Fig. 2a) is first reduced to a 1D equivalent structure (Fig. 2b) by the effective index approach (EIM). The layers of the equivalent slab have the same thickness  $D, H$  and refractive index  $n_i$  of the original structure except the layer containing the core. The refractive index  $n_s$  of this equivalent layer corresponds to the effective index of the slab described by the horizontal cross section of the original layer. In our case it is a silicon slab of thickness  $w$  surrounded by air.

In order to calculate the complex propagation constant of the waveguide, a plane wave  $E_1^+$  incident at an angle  $\phi_1$  from the substrate is considered (Fig. 3). In general almost all the incident power is reflected by the structure, except when the horizontal component of its propagation constant equals the propagation constant of the equivalent slab. In such a case the coupling (i.e. leakage) takes place. The propagation constant  $\beta = k_i \sin \phi_i$  corresponding to the incident angle  $\phi_1$ , is an invariant for the system because of the field continuity at the interfaces.

Within each layer the electric field is the sum of two waves  $E_i^+$  and  $E_i^-$ , propagating respectively in the upward and in the downward directions. Their complex field amplitudes can be calculated by simply multiplying the 2 by 2

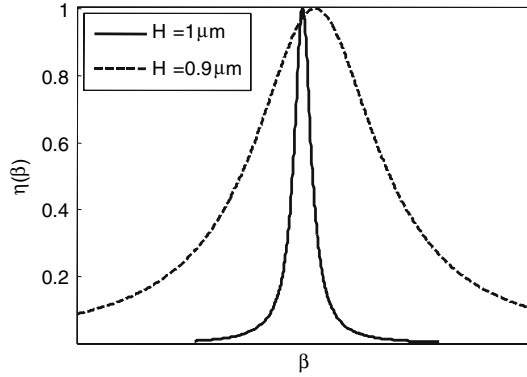


Fig. 4. Excitation efficiency of the TE polarized wave in the core of the silicon on insulator leaky slab of Fig. 1, with  $D=220\text{ nm}$  and  $H=0.9$  and  $1\ \mu\text{m}$ .

transmission matrices  $\mathbf{S}_i$  of each layer as

$$\begin{pmatrix} E_1^+ \\ E_1^- \end{pmatrix} = \mathbf{S}_1 \begin{pmatrix} E_2^+ \\ E_2^- \end{pmatrix} = \dots = \mathbf{S}_1 \mathbf{S}_2 \mathbf{S}_3 \begin{pmatrix} E_4^+ \\ E_4^- \end{pmatrix}$$

where

$$\mathbf{S}_i = \frac{1}{t_i} \begin{pmatrix} e^{j\delta_i} & r_i e^{j\delta_i} \\ r_i e^{-j\delta_i} & e^{-j\delta_i} \end{pmatrix},$$

with  $\delta_2 = n_2 D \cos \phi_2$ ,  $\delta_3 = n_3 H \cos \phi_3$  and  $\delta_1 = 0$  by convenience, and  $r_i$  and  $t_i$  the field reflection and transmission coefficients at the  $i$ th interface. Explicit expressions for both TE and TM polarization can be found in (Ghatak *et al.* 1987)(Tamir).

In case of incidence from the substrate only,  $E_{-4} = 0$ , the excitation efficiency  $\eta(\beta)$  of the electric field in the core results in a Lorentzian shape (Ghatak *et al.* 1987) depending on the incidence angle  $\phi_1$ , or more conveniently on  $\beta = k_1 \sin \phi_1$  as

$$\eta(\beta) = \left| \frac{E_3^+}{E_1^+} \right|^2 \propto \frac{1}{(\beta - \beta_0)^2 + \frac{\alpha^2}{4}}$$

where  $\alpha$  is the full width at half height and  $\beta_0$  its peak position. The efficiencies  $\eta(\beta)$  for a TE polarized incident wave in case of core thickness  $D=0.22\ \mu\text{m}$  and two values of oxide thickness  $H=0.9$  and  $1\ \mu\text{m}$  are shown in Fig. 4. Note that by decreasing the oxide thickness the leakage increases and the Lorentzian shape broadens.

The physical meaning of  $\alpha$  is the power attenuation coefficient of the leaky slab mode, related to the imaginary part of the complex effective refractive index as  $\alpha = 2\pi \Im\{n_{\text{eff}}\}/\lambda$ . The peak position  $\beta_0 = 2\pi \Re\{n_{\text{eff}}\}/\lambda$  is

simply the phase constant of the waveguide mode. Clearly, several peaks are obtained if several modes are supported by the slab.

This method has been used to study the considered waveguide with different oxide thickness and different widths. It has been observed that the proposed method is limited by the confinement factor of the mode in the core rather than by the index contrast. The effective index method that permits the reduction of the original 2D problem to 1D, predicts a more truthful equivalent slab when the mode is strongly confined within the core (Tamir). Figure 5 shows both the real and the imaginary part of the effective index of the Si wire waveguide of Fig. 1 ( $H = 1 \mu\text{m}$ ,  $D = 0.22 \mu\text{m}$ ) as a function of the width  $w$  from  $0.4$  to  $5 \mu\text{m}$ . As a comparison, the results obtained with a commercially available Film Mode Matching technique (FMM) (Fimmwave) are reported as well (more details on the results obtained with this method will be given later). The agreement is fairly good, especially for widths larger than  $0.5 \mu\text{m}$  and both methods tend to the asymptotic slab values. Concerning the imaginary part, the best agreement is found for  $w = 0.5 \mu\text{m}$ , while for wider waveguides the approximated EIM-TMM method slightly overestimates the losses with respect to the FMM. In case of narrow waveguides ( $w < 0.5 \mu\text{m}$ ) losses are underestimated, but in this case the method itself is less accurate due to a weaker mode confinement. A further investigation of the range of validity of the EIM-TMM approach is reported in Fig. 6 where the dependence of the imaginary part of the effective index with respect to the buffer oxide thickness  $H$  and the waveguide width  $w$  is reported. Also in this case results obtained with the FMM are reported and the previous considerations are confirmed independently on the oxide thickness. The calculated effective index of the wire proposed in the COST exercise is  $n_{\text{eff}} = 2.448 - 2.4 \times 10^{-8} j$ .

In conclusion we claim that, although the proposed method is approximate, for the considered Si-wire waveguide it is surprisingly accurate and with all the advantages related to a simple analytical method it is recommended for a first estimation of the complex propagation constant.

### 3. Perturbation theory based on guided mode expansion

The idea of this approach is to calculate propagation losses due to leakage in the substrate by perturbation theory: the zero-order structure has a semi-infinite  $\text{SiO}_2$  lower cladding and it supports truly guided modes, while the dielectric perturbation  $\Delta\varepsilon(\mathbf{r}) = (\varepsilon_4 - \varepsilon_3)\theta(-z - h)$  leading to loss occupies the lower silicon layer and consists of the difference between the dielectric constants of silicon ( $\varepsilon_4$ ) and of  $\text{SiO}_2$  ( $\varepsilon_3$ ), as sketched in Fig. 7. Furthermore, the silicon wire is repeated with supercell periodicity  $W + W'$  in the  $x$  direction.

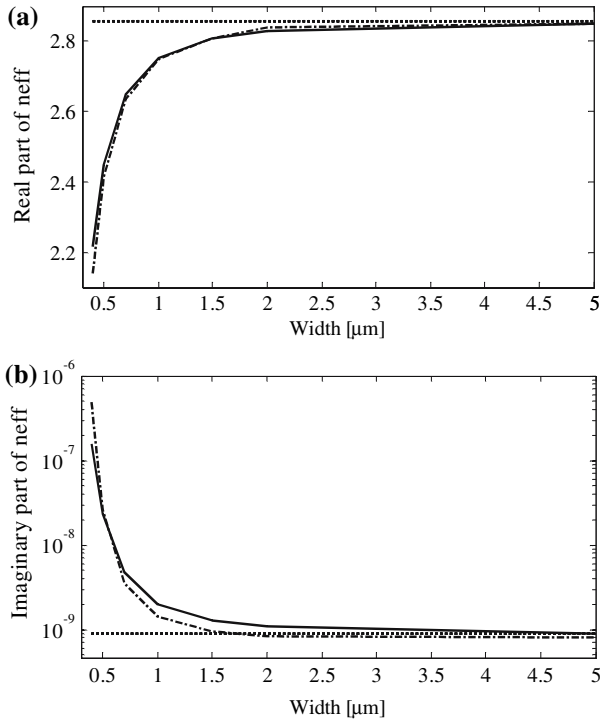


Fig. 5. (a) Real and (b) imaginary part of the effective index of the Si wire waveguide of Fig. 2 ( $D = 1 \mu\text{m}$ ,  $H = 0.22 \mu\text{m}$ ) vs. waveguide width. EIM-TMM (solid line), FMM [3] (dash-dot). The asymptotic line (dots) refers to the slab.

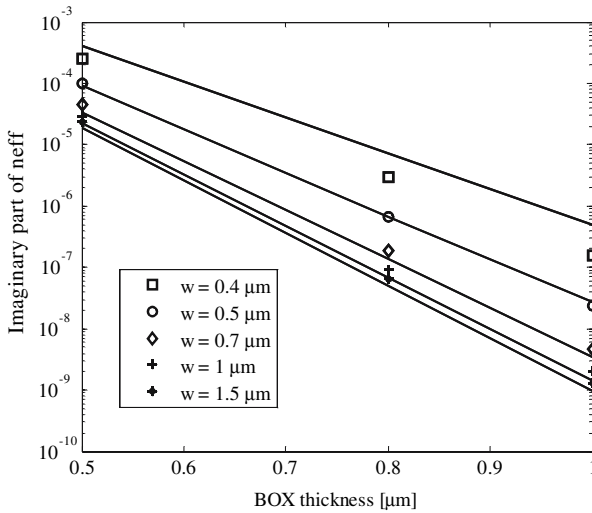


Fig. 6. Imaginary part of the effective index of the Si wire waveguide of Fig. 2 for different widths  $w$  and buffer oxide thicknesses. EIM-TMM (marks); commercial FMM (solid line).

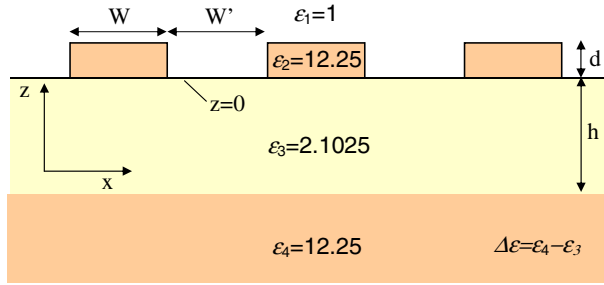


Fig. 7. Schematic layout of the Silicon wire structure repeated periodically along the  $x$  direction. The dielectric perturbation for the loss calculation extends over layer 4 and it consists of the difference in dielectric constants between Silicon ( $\epsilon_4 = 12.25$ ) and  $\text{SiO}_2$  ( $\epsilon_3 = 2.1025$ ).

The photonic mode dispersion in the structure with semi-infinite  $\text{SiO}_2$  is calculated by a guided-mode expansion method (Andreani and Gerace 2006), which consists of expanding the magnetic field in the basis of guided modes of an effective homogeneous waveguide with an average dielectric constant in each layer. The method is a fully vectorial one. Satisfactory results are obtained using  $W' = W$  (i.e., the supercell period is twice the wire width), one guided mode in the basis, and 21 plane waves. The dispersion of the lowest-order TE mode and the corresponding effective index are shown in Fig. 8a and b, respectively. The effective index at an energy  $E = 0.8 \text{ eV}$  (corresponding to the target wavelength  $\lambda = 1.55 \mu\text{m}$ ) is  $\text{Re}(n_{\text{eff}}) = 2.35$ . Propagation losses are calculated by perturbation theory, with a formalism similar to that of (Andreani and Gerace 2006). The relevant formula is

$$\text{Im}(k) = \frac{\pi \omega^2}{4v_g} \left| \int \mathbf{E}_{\text{guided}}(\mathbf{r})^* \cdot \mathbf{E}_{\text{rad}}(\mathbf{r}) \Delta \epsilon(\mathbf{r}) d\mathbf{r} \right|^2 \rho(\omega),$$

where  $\mathbf{E}_{\text{guided}}$  ( $\mathbf{E}_{\text{rad}}$ ) is the electric field of a guided (radiation) mode of the effective waveguide,  $\rho(\omega)$  is the photonic density of states for a given wavevector in the  $xy$  plane and  $v_g = d\omega/dk$  is the mode group velocity. Notice that for the present case of TE polarization and one guided mode in the basis, both guided and radiation modes have an electric field which is parallel to the interface between layers 3 and 4, thus the field components are continuous across the interface and the perturbative formula is unaffected by corrections due to shifting boundaries (Johnson *et al.* 2002). The imaginary part of the effective index  $\text{Im}(n_{\text{eff}}) = c\text{Im}(k)/\omega$  is shown in Fig. 8c as a function of frequency for three different values of the  $\text{SiO}_2$  thickness  $h$ . The values are very small, thereby justifying the use of perturbation theory. The losses decrease exponentially with increasing frequency and  $\text{SiO}_2$  thickness: the dependence is  $\text{Im}(n_{\text{eff}}) \propto \exp(-2\chi_3 h)$ , where

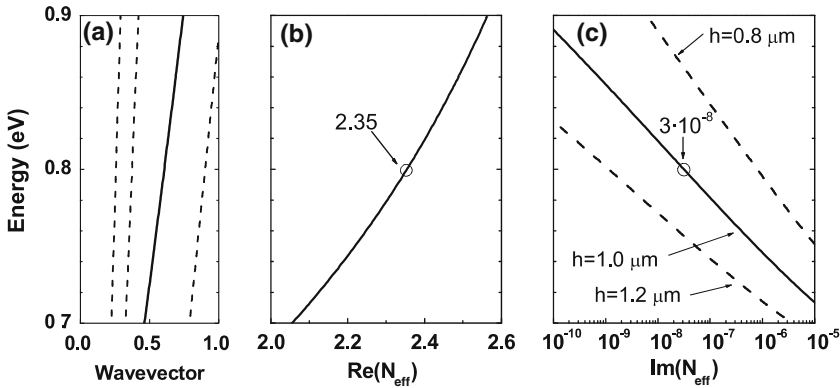


Fig. 8. (a) Dispersion of the fundamental TE mode of the Si wire (solid line) and light lines in the core and cladding materials (dashed lines); (b) real part of the effective index; (c) imaginary part of the effective index for three different values of the SiO<sub>2</sub> layer thickness.

$$\chi_3 = (k^2 - \varepsilon_3 \omega^2 / c^2)^{1/2} = (\text{Re}(n_{\text{eff}})^2 - \varepsilon_3)^{1/2} (\omega / c)$$

is the imaginary part of wavevector in the SiO<sub>2</sub> cladding. The loss value for  $h = 1 \mu\text{m}$  and  $E = 0.8 \text{ eV}$  is  $\text{Im}(n_{\text{eff}}) = 3 \cdot 10^{-8}$ , in fair agreement with the results obtained with the other methods.

The advantages of the present perturbative approach are its computational efficiency and ease of application for different frequencies and structure parameters. The disadvantage is that it is difficult to get accurate numbers, especially for  $\text{Re}(n_{\text{eff}})$ , because of the supercell representation of the silicon wire structure. In order to improve the accuracy of the results and to avoid introducing a supercell, the perturbative calculation of losses could be built upon a numerical solution for the guided mode of a single photonic wire, as obtained e.g. with other approaches described in this paper.

#### 4. Beam propagation method

The beam propagation method (BPM) has been considered to be one of the most useful and flexible techniques used to study the evolution of light waves along longitudinally variant and invariant waveguiding structures. However, the combination of the BPM with the imaginary distance propagation technique (IDBPM) has been proved recently to be a very useful “mode solver” for various optical waveguides (Xu *et al.* 1993; Wijnands *et al.* 1994; Tsuji and Koshiya 2000). The idea is simply that if an arbitrary initial field is allowed to propagate along, in general, a complex axis, with the selection of the proper propagation step size, a sequence of different modes, starting from the fundamental, can be extracted from the initial

field. Besides the elegance of the IDBPM in finding the modes in a sequential way, it has no additional computation burden in dealing with the complex modes existing either in lossy (or with gain) structures or leaky-mode waveguides, as the original BPM matrices are complex.

However, most the IDBPM approaches reported in the literature are based on the formulation of the less accurate, and yet simpler, scalar wave approximation. Recently, we have presented the combination of the full vectorial finite element based BPM with the imaginary distance technique (IDVFEBPM) (Obayya *et al.* 2002) as an efficient and accurate modal solution approach for different optical waveguides. This formulation is based on the use of the transverse magnetic field components, it being not only numerically efficient as it solves for only two, rather than the full three field components, but also totally eliminates the possibility of the appearance of spurious modes in the solution via the rigorous inclusion of the zero divergence and the interface boundary conditions using an elegant line integration approach (Obayya *et al.* 2000). Also, to deal effectively with waveguiding structures involving radiation and leaky modes, the perfectly matched layer (PML) has been incorporated in the formulation so as to be capable of accounting for leaky modes such as those in the waveguide problem in hand. In our formulation, the conventional PML boundary condition has been used, and its conductivity profile is given as (Obayya *et al.* 2000)

$$\alpha = 1 - j \frac{3\lambda\rho^2}{4\pi n_{\text{tr}} W_{\text{PML}}^3} \ln(1/R) \quad (1)$$

where  $\lambda$  is the wavelength,  $n_{\text{tr}}$  is the transformed index of refraction,  $W_{\text{PML}}$  is the width of the PML layer,  $\rho$  is the distance inside the PML layer from its interface with the computational window and  $R$  is the theoretical reflection coefficient placed at the interface between the computational window and the PML layer. Although IDVFEBPM is an efficient mode solver, it may suffer, in very few cases, in finding the desired mode. In this case, an initial guess that is close to the mode effective index can greatly enhance the speed of convergence to the desired mode.

We have investigated the convergence of our model as a function of two parameters: the reflectivity  $R_{\text{PML}}$  of the PML and the thickness  $H$  of the substrate before it reaches the bottom PML. The results are summarized in Tables 1 and 2.

## 5. Finite element method (H. Uranus)

The method used to calculate the modes in this work is a finite element method (FEM) leaky mode solver using a 1st-order Bayliss-Gunzburger-Turkel-like

Table 1. Convergence of the IDVFEBPM for different values of  $H$  using  $R_{\text{PML}} = 10^{-30}$ 

$H$ ( $\mu\text{m}$ )	$\text{Re}(n_{\text{eff}})$	$\text{Im}(n_{\text{eff}})$
0.75	2.413340	$-j 3.923 \times 10^{-8}$
1.05	2.413340	$-j 3.720 \times 10^{-8}$
1.55	2.413340	$-j 2.319 \times 10^{-8}$
2.15	2.413340	$-j 2.831 \times 10^{-8}$
2.65	2.413340	$-j 3.020 \times 10^{-8}$
3.15	2.413340	$-j 2.694 \times 10^{-8}$

Table 2. Convergence of the IDVFEBPM for different values of  $R_{\text{PML}}$  using  $H = 3.15 \mu\text{m}$ 

$R_{\text{PML}}$	$\text{Re}(n_{\text{eff}})$	$\text{Im}(n_{\text{eff}})$
$10^{-5}$	2.413340	$-j 2.758 \times 10^{-8}$
$10^{-10}$	2.413340	$-j 2.823 \times 10^{-8}$
$10^{-15}$	2.413340	$-j 2.843 \times 10^{-8}$
$10^{-20}$	2.413340	$-j 2.809 \times 10^{-8}$
$10^{-25}$	2.413340	$-j 2.754 \times 10^{-8}$
$10^{-30}$	2.413340	$-j 2.694 \times 10^{-8}$

(BGT-like) boundary condition (BC). The details of the method have been given in (Uranus *et al.* 2004).

The structure is discretized by a mesh of unstructured triangular elements. Using a Galerkin procedure, a discretized weak form of the vectorial wave equation, expressed only in terms of transverse components of the magnetic field, is formulated. By approximating the field within each triangular element using interpolation of nodal-based quadratic basis functions and handling the field and its derivatives at the computational boundary using appropriate boundary conditions, a generalized matrix eigenvalue equation is obtained and solved for the complex-valued effective indices and the associated modal fields. At computational boundaries where the field is expected to pass with low reflection, the normal derivative operator of the field is approximated using a Dirichlet to Neumann map formulated using a 1st-order BGT-like BC.

After exploiting mirror symmetry of the structure, the computational window has a width of  $1 \mu\text{m}$ . Its total height is  $2.5 \mu\text{m}$  with the substrate taking  $0.5 \mu\text{m}$ . To reduce the discretization error, we intentionally refine the mesh elements in the vicinity of the core, in the buffer layer, along the interfaces of the core, and in the vicinity of the corners. However, this simple mesh refinement procedure is not an adaptive mesh refinement yet. Figure 9 shows an example of the mesh for one of the computational settings.

The computational results are shown in Table 3 for various mesh refinement settings. The structure is effectively single mode with very low leakage loss for the fundamental quasi-TE mode and highly leaky other modes. Note that highly leaky modes are automatically filtered out during the

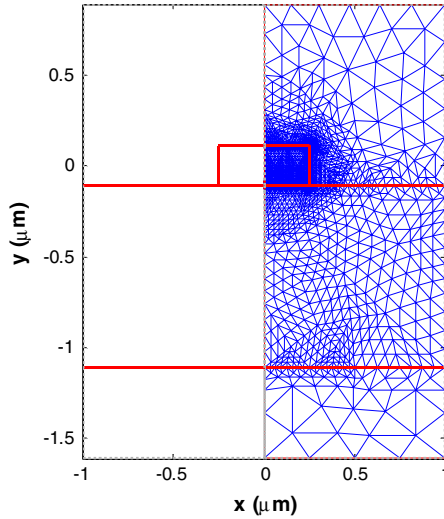


Fig. 9. The mesh for discretization with 9463 triangular elements.

computations. The results show that it is hard to get accurate effective indices for this particular structure. We suspect that this is caused by the insufficient handling of corners and the insufficient fulfillment of continuity of  $\partial_x H_x + \partial_y H_y$  (which in our code is approximately satisfied through weighted average of evaluation of derivatives of two triangular elements sharing the same line element at the interface) while evaluating line integral along interfaces in our nodal-based FEM formulation. Since the field is rather strong near the corners and at interfaces, the error caused by insufficient handling of corners and interfaces will be significant. It is clear that a finer mesh is indeed required for better results, but unfortunately it is already at the limits of the memory capacity of our workstation. The computed effective index for the mode lies between  $2.4131-2.97 \times 10^{-8} j$  and  $2.4132-2.97 \times 10^{-8} j$ .

For the 1st computation (9463 triangular elements), the typical computation time is 161 s for preprocessing (mesh generation and matrices assembling) and 685 s for mode searching on our P4-2GHz IGB computer using Matlab 6.1 and MS-XP-Pro operating system. For this initial computation, we have chosen a scheme that first used homogeneous Dirichlet BC to generate many initial guesses of  $n_{\text{eff}}$  located between 3.5 and 1.45, then searched for leaky modes (using the 1st-order BGT-like BC) near to these initial guesses and automatically picked up only modes with low attenuation. This mode searching scheme is not efficient because many rather irrelevant leaky modes (due to the fact that leaky structures are always highly multimoded) have to be calculated before reaching the modes of interest, but reduces

Table 3. Results for the fundamental mode by refining the mesh

Meshes		$n_{\text{eff}}$	
Triangular elements	Nodes	Real	-imaginary
9463	19022	2.413430	2.9533E-8
9570	19255	2.413607	2.9436E-8
11933	24014	2.413429	2.9566E-8
14492	29179	2.413218	2.9622E-8
15291	30792	2.413290	2.9611E-8
18774	37777	2.413437	2.9575E-8
20050	40331	2.413249	2.9626E-8
24422	49101	2.413125	2.9651E-8
25306	50883	2.413130	2.9667E-8
25397	51048	2.413200	2.9641E-8
25801	51876	2.413130	2.9668E-8

the possibility to miss the modes. To reduce the computational time, for the rest of the results in Table 3, we have chosen a scheme that used the  $n_{\text{eff}}$  of the 1st computation as an initial guess, and searched only for  $n_{\text{eff}}$  near to this value. This scheme reduces the mode searching time to 191 s with 170 s preprocessing time for the 2nd computation (9570 triangular elements). For the computation with finest mesh (25801 triangular elements), it takes 973 s for the preprocessing and 1062 s for the mode searching. If we need to calculate  $n_{\text{eff}}$  for nearby wavelengths (even by taking material dispersion into account), the preprocessing time can be reduced to a negligible time, because it is not necessary to regenerate the mesh, hence most components that compose the matrices of the previous computation can be reused.

## 6. Finite element method (S. Selleri)

The analysis of the wire waveguide has been performed using the finite element method. This method is very powerful as it can cope with any kind of geometry and medium characteristic and can provide a full-vectorial analysis which is necessary to model waveguides with large index variations.

Our formulation of the FEM is based on the curl-curl equation and the related functional expression (Selleri and Petracek 2001; Selleri *et al.* 2001). The domain under investigation has been discretized using high order triangular edge elements, with six tangential unknowns and two inner normal ones, which avoid the presence of spurious modes in the solution spectrum. Both electric and magnetic field based formulations can be derived. By discretizing the functional and by looking for its stationary point, an eigenvalue algebraic problem is obtained whose matrices are sparse

and symmetric. The algebraic problem can be resolved by means of the ARPACK library based on the Arnoldi method (ARPACK) which can efficiently provide few dominant eigenvalues and eigenvectors, corresponding to the fundamental and first higher order modes of the waveguide. The eigenvalues provide the complex propagation constant, while the eigenvectors give the mode vectorial field distribution.

An Anisotropic Perfectly Matched Layer (PML) is placed before the outer boundary to enclose the computational domain and avoid undesired reflection from the computational domain border (Cucinotta *et al.* 1999). The cladding-PML interface is reflectionless independent of polarization, frequency and direction of the impinging wave. Its absorbing properties are a function of the conductivity profile  $\sigma$ . In particular it can vary all over the layer width from zero at the cladding-PML interface, to a maximum value  $\sigma_{\max}$  on the outer boundary, following an  $m$ -power profile:

$$\sigma = \sigma_{\max}(\rho/d)^m,$$

$\rho$  and  $d$  being, respectively, the distance from the beginning of the PML layer and its width. Different  $m$  values provide different conductivity profiles within the anisotropic layer.

When looking for solutions affected by field leakage, as in the case of the considered structure where the substrate presents the same refractive index as the waveguide, the choice of the PML parameters is very important and a convergence analysis is mandatory to verify the results reliability. Besides PML, many other parameters, mainly mesh distribution, number of sampling points or element type, affect the solution accuracy and deserve to be investigated. For the sake of brevity this analysis has not been reported and the attention is focused on the effect of the PML parameters.

The width  $d$  has been assumed equal to 1, 2 and 3  $\mu\text{m}$  while typical values of  $m$  were 2, 3 or 4. These values affect the speed with which the real and imaginary part of the propagation constant converge to the final result and, to a certain degree, the final results itself, as they define the conductivity profile within the PML as a function of  $\sigma_{\max}$ . By increasing  $\sigma_{\max}$ , it is possible to achieve stable values for the propagation constant, which can however slightly vary according to the different combination of the parameters. Some examples are reported in Table 4 for the fundamental TE mode by considering the PML width equal to 1  $\mu\text{m}$  and 3  $\mu\text{m}$  and the parabolic ( $m = 2$ ) and cubic ( $m = 3$ ) conductivity profile. Notice that while convergence of the real part is easily obtained, a unique value of the imaginary part has not been achieved, in spite of the huge variety of parameter combinations. However the most reliable convergence behaviour is given with  $d = 1 \mu\text{m}$  and  $m = 3$ , providing a value of  $2.45 \times 10^{-8}$ .

Table 4. Convergence of FEM mode solver of Parma University

Parma University FEM Modal Solver			real $n_{\text{eff}}$	imag $n_{\text{eff}}$
$d = 1 \mu\text{m}$	$m = 2$	$\sigma_{\text{max}} > 10^9$	2.41232	$0.22 \times 10^{-8}$
$d = 1 \mu\text{m}$	$m = 3$	$\sigma_{\text{max}} > 10^9$	2.41232	$2.45 \times 10^{-8}$
$d = 3 \mu\text{m}$	$m = 2$	$\sigma_{\text{max}} > 10^{11}$	2.41233	$0.95 \times 10^{-8}$
$d = 3 \mu\text{m}$	$m = 3$	$\sigma_{\text{max}} > 10^{11}$	2.41233	$3.90 \times 10^{-8}$

The solver is implemented in FORTRAN in a Linux environment, with a simple command-line interface, yielding the three components of the magnetic field vector on the whole structure. It can also simulate half- and quarter-structures, by placing PEC and PMC boundary conditions on the boundaries representing the symmetry axes. It can operate an automatic search for the eigenvalues, or an estimate can be manually supplied to speed up convergence. On a 2.4-GHz Pentium 4 PC with 2 GB of RAM, calculation time for one eigenvalue at one frequency is about one minute, while the maximum number of mesh nodes ranges from 45000 to 55000 depending on structure complexity.

## 7. Olympios

The real and the imaginary part of the effective index of the fundamental quasi-TE mode of the photonic wire were calculated using a commercially available finite difference mode solver: Olympios from C2V (Olympios). Their so-called ‘‘FD Generic’’ solver is based on the well-known finite difference method, initially solving Maxwell’s equations in terms of the transversal magnetic field  $H(x, y)$ , using a staggered grid. This full vectorial complex mode solver uses PML boundary conditions. The strength of the PML-layers can be adjusted. These settings have been optimized for convergence before performing the final calculations presented here. The settings were chosen as follows:

The number of grid points used within the PMLs is proportional to the total number of grid points, i.e. a grid of  $100 \times 100$  results in an effective grid of  $70 \times 70$ , with 15 grid points in PML layers on both sides. The size of the calculation was set to 4 by 4 micrometer to make sure that the tail of the field has dropped in the horizontal direction to almost zero ( $>50$  dB drop).

The grid size was varied from  $50 \times 50$  to  $375 \times 375$  (i.e. 2500–140625 points). Both a uniform and a non-uniform grid were used. The upper value of the grid size is limited by the maximum size of the memory allocation by Olympios and not by the size of the physical memory.

Table 5. Numerical parameters used in the Olympios simulations

Parameter	value
<b>PML Reflectivity</b>	$1 \times 10^{-100}$
<b>Number of PML points</b>	<b>15</b>
<b>Maximum number of iterations</b>	<b>10</b>
<b>Maximum iteration depth</b>	$1 \times 10^{-10}$

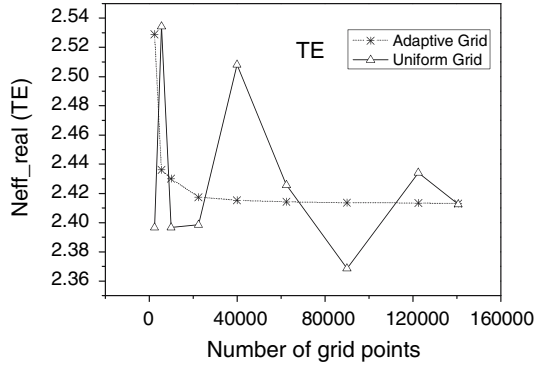


Fig. 10. The real part of the effective index versus the (total) number of grid points for both grid types.

Figure 10 shows the calculation results for the real part of the effective index. It is clear that the adaptive grid performs much better than a uniform grid in all cases. The real part converges to 2.413, for the adaptive grid. The value of the imaginary part, shown in Fig. 11, converges to  $2.9 \times 10^{-8}$ .

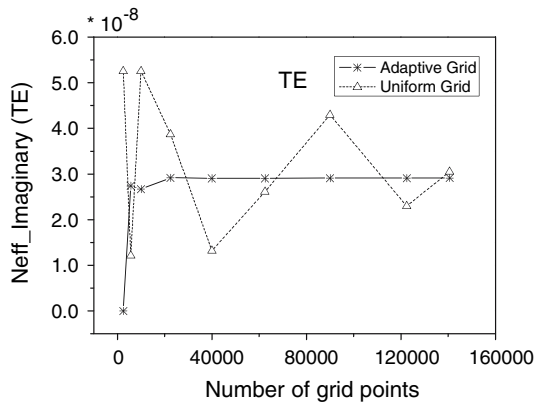


Fig. 11. The imaginary part of the effective index versus the (total) number of grid points for both grid types.

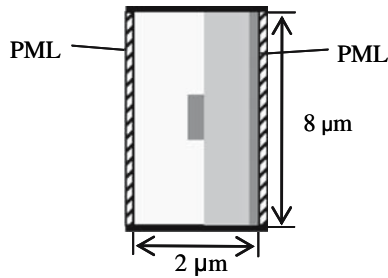


Fig. 12. The structure simulated by FMM with emphasis on the dimension of the computational window and on the boundary conditions: metallic walls (black) and PMLs (dashed).

With the adaptive grid, both the real and imaginary part show a smooth behaviour as function of the number of grid points ( $> 20000$ ), which suggests that a higher number of grid points may result in more accurate values for both parts, although a systematic error cannot be excluded.

The real part of the effective index could be calculated with 4 digits accuracy. The imaginary part could be determined with only 2 digits accuracy. However, if the program would be able to handle a larger number of grid points, a possible better convergence is expected.

## 8. Fimmwave

The complex propagation constant of the photonic wire has been calculated by a commercially available tool based on the Film Mode Matching method (FMM): Fimmwave by Photon Design (Fimmwave).

The algorithm of this complex vectorial solver starts by dividing the rectangular computational windows into a number of suitable sections. The field inside each section is described by a mode expansion (Sudbo 1993) and the field continuity is imposed at the interfaces. The whole structure is enclosed in a computational box and the boundary conditions on the walls can be chosen between electric, magnetic and PML. For an accurate simulation, there are several key parameters requiring a convergence analysis, in particular the dimensions of the computational window, the number of modes in each section (1D modes) and the PML thickness.

The details of the simulated structure are reported in Fig. 12: the structure has been rotated by  $90^\circ$  because of some constraint of the simulator (ver. 4.4), the PMLs are placed only laterally while upper and bottom boundaries are electric walls. The window dimensions have been chosen to be 2 by  $8 \mu\text{m}$  after a simple convergence analysis. Moreover, it has been noted that in some rare cases the computational algorithm failed to converge.

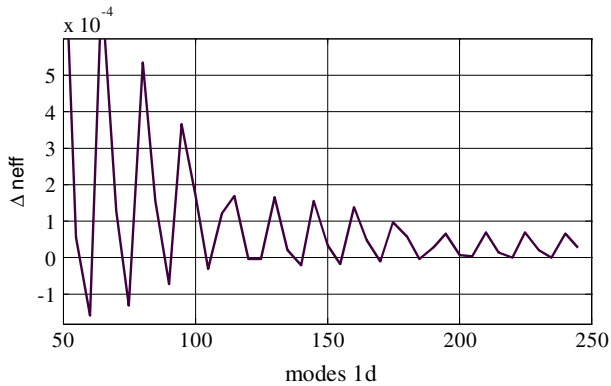


Fig. 13. Convergence of the real part of the propagation constant vs. the number of 1D modes.

The strength of the PMLs can be controlled by adjusting the thickness of the layers. The algorithm results are quite stable with respect to this parameter, the results converging to the same value for PMLs thickness larger than few tenths of micron. A thickness of  $1\ \mu\text{m}$  was conservatively chosen.

Relating to the 1D modes, the larger the number, the more accurate are the results. Fig. 13 reports the convergence analysis performed on the real part of the propagation constant. Even with a large number of 1D modes an oscillating behaviour was found, with an uncertainty better than  $6 \times 10^{-5}$  achieved for more than 200 modes. The results obtained for the quasi-TE fundamental mode of the analysed waveguide is  $n_{\text{eff}} = 2.41235 - 2.688 \times 10^{-8}j$ . The computational time for the problem discussed with 200 modes 1D is around 600 seconds on a standard 1 GHz computer, and drops to less than 100 seconds with 120 modes.

## 9. Film mode matching (P. Bienstman)

In this modelling method, the wire is subdivided into a number of horizontal slices. In each of these slices, the field is expanded in the local eigenmodes of that particular layer, which are being rotated in such a way that they all have the same wavevector component  $k_z$  in the propagation direction (Bienstman 2004).

Note that in order to model this particular structure, metal walls are only being placed at the left and right side of the structure, whereas the top and bottom edges are infinitely extended (see Fig. 14), as the algorithm allows for treating open space analytically along a single propagation direction. Indeed, in order to be able to use eigenmode expansion with the 1D slab

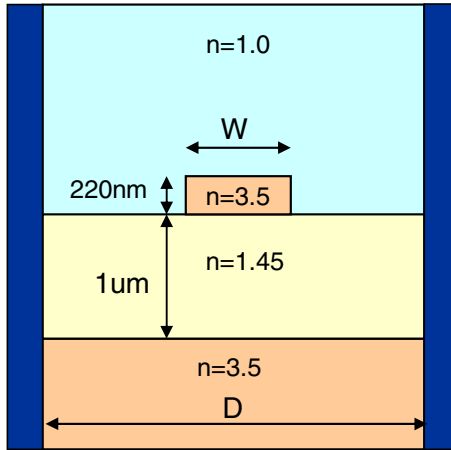


Fig. 14. Boundary conditions used in UGent's film mode matching method.

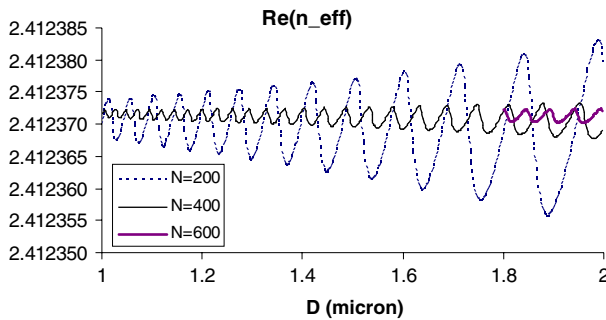


Fig. 15. Real part of the effective index as a function of distance between the walls for different numbers of 1D modes (note that the  $N = 600$  curve is only shown from  $D = 1.8 \mu\text{m}$ ).

eigenmodes, it is only needed that these 1D modes form a discrete set, which is the function of the metal walls to the left and the right of the structure. The fact that the structure is still open to the top and the bottom means that some modes of the 2D cross section will form continuous sets. However, that is not important if we are just interested in the guided modes of the wire.

This means that there are only two parameters that need to be varied in order to check the convergence of the method: the distance between the two vertical metal walls and the number of eigenmodes retained in the series expansion.

Figures 15 and 16 show the real and the imaginary part of the effective index as a function of the distance  $D$  between the walls, and this for different number  $N$  of 1D modes.

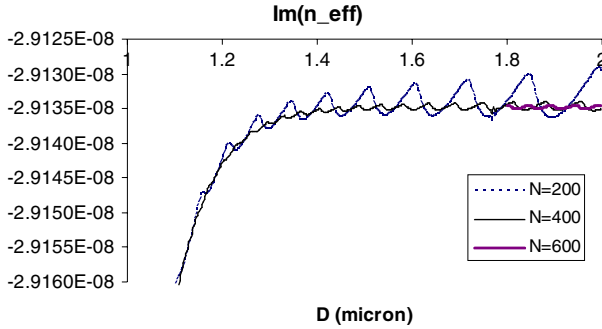


Fig. 16. Imaginary part of the effective index as a function of distance between the walls for different numbers of 1D modes (note that the  $N = 600$  curve is only shown from  $D = 1.8 \mu\text{m}$ ).

From Fig. 16 one can see that after a distance of 1.5 micron, the loss stabilises. Therefore, the residual oscillations in Fig. 15 are not due to parasitic reflections, but rather they decrease as the number of 1D modes is increased. From the calculations with  $N = 600$ , one can deduce a stable value of  $n = 2.412372 - 2.9135 \times 10^{-8} j$ . However, at 600 modes calculating a single data point already represents a considerable numerical effort (around 2 hours on a 2 GHz computer). Using 200 modes, this drops to 100 seconds.

The implementation of the method is freely available in the software tool CAMFR (CAMFR).

### 10. Aperiodic Fourier Modal Method

The Aperiodic Fourier Modal Method (A-FMM) used in this work can be referred to as a fully-vectorial “transverse resonance method” following the classification in (Vassallo 1997). For the specific problem considered here, it has been described in a previous publication (Hugonin *et al.* 2005) and has been successfully benchmarked for the calculation of the real propagation constant of ridge waveguides. We will not repeat here the details of the method and will just summarize the main important issues. In brief, the principles of the method originate from a generalization of classical grating methods known as the Rigorous-Coupled-Wave-Analysis or the Fourier Modal Method (Moharam *et al.* 1995), to handle aperiodic geometries through an artificial periodization and through the use of perfectly-matched layers (Silberstein *et al.* 2001). The method relies on an analytical integration along the  $y$ -direction, and on the use of a nonlinear real coordinate transform (Hugonin and Lalanne 2005) which maps the two semi-infinite (open) intervals of the Cartesian  $x$ -axis to finite intervals of width  $q$  in a new coordinate axis  $x'$ , see Fig. 17. Because the waveguide modes predom-

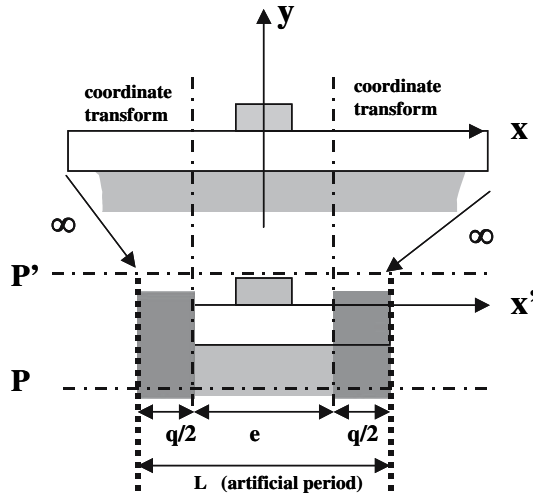


Fig. 17. Schematic representation of the artificial periodizations used in this work and illustration of the non-linear transform used for mapping the semi-infinite real spaces  $|x| > e/2$  onto finite real spaces  $e/2 < |x'| < e/2 + q/2$ .

inantly leak in the direction of the substrate, the fields are very close to zero at the lateral boundaries of the computational box. They are thus periodic functions of the  $x'$ -coordinate and can be expanded in Fourier series. This introduces an artificial “periodization” along the  $x'$  coordinate, virtually replacing the actual waveguide isolated in space by a one-dimensional periodic waveguide grating. Although the artificial period  $L$  is finite in the new space  $x'$ , the distance between adjacent waveguide in real space is indeed infinite.

The analytical integration along the  $y$ -direction in Fourier space is performed with classical scattering S-matrix algorithms (Li 1996) which links the Fourier-expansion coefficients of the transversal  $x'$ - and  $z$ -components of the electromagnetic fields in two planes perpendicular to the  $y$ -axis and located in the upper (air) and lower (silicon) claddings. These planes are denoted  $P$  and  $P'$  in Fig. 17. For a parallel momentum ( $k_{x'} = 0, k_z$ ), a situation usually referred to as purely-conical diffraction in grating theory (the plane of incidence is parallel to the grooves), the complex effective index  $n_{\text{eff}}$  is seen as the complex pole  $k_z = k_0 n_{\text{eff}}$  of  $\mathbf{S}$ . In principle, arbitrary accuracy can be achieved by increasing the number of Fourier harmonics retained in the field expansion. In practice, the Fourier expansion have to be truncated and we denote the truncation rank by  $M_x$ ,  $2M_x + 1$  being the total number of Fourier harmonics retained for the computation. As  $M_x$  increases, limitations may arise from memory requirements, or from the finite precision of the numerical calculations which essentially rely on

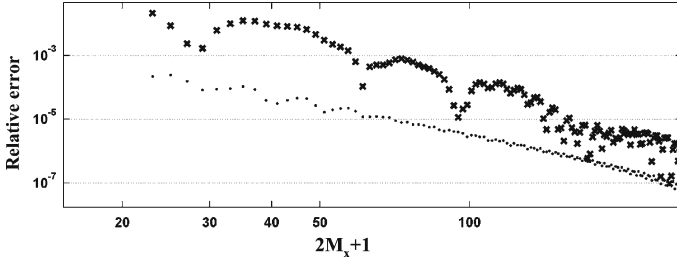


Fig. 18. Convergence performance of the Fourier modal method as a function of the total number of Fourier harmonics for  $q = 0.3\mu\text{m}$  and for  $e = 0.5\mu\text{m}$ . The relative error is defined as  $|\text{Re}(n_{\text{eff}} - n_0)|/\text{Re}(n_0)$  (dots) for the real part of the effective index and as  $|\text{Im}(n_{\text{eff}} - n_0)|/\text{Im}(n_0)$  (crosses) for the imaginary part of the effective index, where  $n_{\text{eff}}$  is the effective index calculated for a given  $M_x$  and  $n_0 = 2.412372039 + i2.9134801 \times 10^{-8}$  is the effective index value extrapolated for  $M_x \rightarrow \infty$ .

matrix diagonalization and multiplications. We used a Padé-like algorithm for the pole calculation, the root search being performed with less than 4 iterations, starting from an initial guess value calculated with a small  $M_x$  value.

The convergence performance of the method is shown in Fig. 18. As the total number  $2M_x+1$  of Fourier harmonics retained for the calculation increases, the relative error defined in the figure caption rapidly decreases. All the calculations are performed on a PC computer equipped with a 3-GHz processor and with a Matlab 7 software. In Fig. 18, the results are obtained for  $q = 0.3\mu\text{m}$  and for  $e = 0.5\mu\text{m}$ , see Fig. 17 for a definition of these numerical parameters. We have performed other calculations for other values of  $q$  and  $e$ . By varying  $q$  by one-order of magnitude from  $0.2\mu\text{m}$  to  $2\mu\text{m}$  and  $e$  from  $0.5\mu\text{m}$  to  $1.5\mu\text{m}$ , the numerical results obtained for  $M_x = 400$  exhibit stable properties. In particular the 7-first digits of  $\text{Re}(n_{\text{eff}})$  and the 6-first non-null digits of  $\text{Im}(n_{\text{eff}})$  are stabilized and equal to  $2.4123720 \pm 2 \times 10^{-7}$  and  $2.913480 \pm 2 \times 10^{-6}$ , respectively. We found that the best convergence performance is achieved for  $e \approx q \approx 0.5\mu\text{m}$ . Typical CPU-times for the computation of the effective index with  $2M_x + 1 = 61$  (resp. 301) is approximately 16 (resp. 240) seconds on a PC computer equipped with a 2.8-GHz processor and with Matlab software. Finally, let us mention that the coordinate-transform, which maps the semi-infinite open space to real axes in this work, can be also implemented with a small modification in the complex plane. In that case, both guided and radiated modes can be computed, and classical scattering problems in integrated-optics can be efficiently analysed by handling light radiation into the claddings through the complex mapping (Hugonin and Lalanne 2005).

## 11. Plane wave admittance method

The plane-wave admittance method (Dems *et al.* 2005) is a universal method for optical analysis of multi-layered structures. The method has been verified to be a reliable tool for analysis of band structure of photonic crystal slabs (Dems *et al.* 2005) eigenmodes of photonic waveguides or vertical cavity surface emitting lasers (VCSELs) (Dems and Panajotov 2006; Dems *et al.* 2006) (Czyszanowski *et al.* 2006). Its main idea is that the solution is obtained analytically along one axis with numerical plane-wave expansion in the remaining directions. In the case of longitudinally invariant waveguide only a one-dimensional numerical expansion is necessary. The main difference between this method and the one presented previously is the different algorithm of obtaining the analytical solution along the  $y$ -axis. In plane-wave admittance method we use the admittance transfer technique, which does not suffer any instabilities even for the very thick layers (Conradi *et al.* 2001).

$$\begin{aligned} \partial_z \begin{bmatrix} -E_y \\ E_x \end{bmatrix} &= -j \frac{\eta_0}{k_0} \begin{bmatrix} \partial_y \varepsilon_z^{-1} \partial_y + \mu_x k_0^2 & -j\beta \partial_y \varepsilon_z^{-1} \\ -j\beta \varepsilon_z^{-1} \partial_y & -\beta^2 \varepsilon_z^{-1} + \mu_y k_0^2 \end{bmatrix} \begin{bmatrix} H_x \\ H_y \end{bmatrix} \\ \partial_z \begin{bmatrix} H_x \\ H_y \end{bmatrix} &= -j \frac{\eta_0}{k_0} \begin{bmatrix} -\beta^2 \mu_z^{-1} + \varepsilon_y k_0^2 & j\beta \mu_z^{-1} \partial_x \\ j\beta \partial_y \mu_z^{-1} & \partial_y \mu_z^{-1} \partial_y + \varepsilon_x k_0^2 \end{bmatrix} \begin{bmatrix} -E_y \\ E_x \end{bmatrix} \end{aligned}$$

where  $k_0 = 2\pi/\lambda$  is normalized frequency,  $\beta = n_{\text{eff}} k_0$  is the propagation constant,  $\varepsilon$  and  $\mu$  are anisotropic permittivity and permeability and  $E_x$ ,  $E_y$ ,  $H_x$  and  $H_y$  represent electromagnetic field components parallel to the layers of the structure. In the case analysed in this article  $x$  is the direction of the propagation of light, and  $z$  is perpendicular to the wire and the substrate. The equations above can be solved analytically provided they are represented in some finite matrix form and transformed to new coordinates in which resulting matrix is diagonal. The eigenmodes are determined with admittance transfer procedure (Conradi *et al.* 2001; Dems *et al.* 2005). In the plane-wave admittance method the numerical representation of the above matrices is obtained by representing the fields in finite plane-wave basis. The truncation of the computational domain is achieved with uniaxial perfectly matched layers (UPML) represented by diagonally anisotropic permittivity and permeability tensors. This allows for the analysis of infinite structures without modifying the equations.

The modelled structure is presented in Fig. 19. We used 6 layers, the top and bottom of which are PMLs, and the rest being air, a layer containing the wire itself, the oxide and the substrate. The thickness of the top PML, the air and the substrate was 4, 4 and  $8 \mu\text{m}$ , respectively.

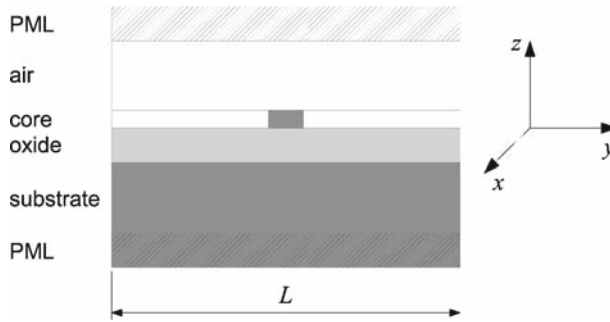


Fig. 19. Definition of the geometric parameters of the plane wave admittance method.

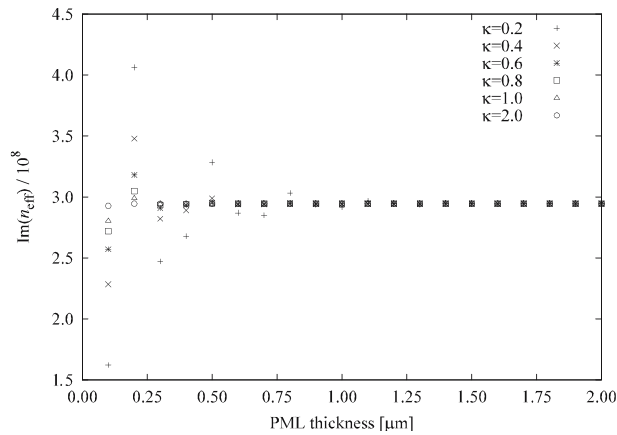


Fig. 20. The dependence of the imaginary part of the effective index on the PML thickness for different PML absorptions. The refractive index of the layer is a diagonal tensor of the form  $n = n_0 \text{diag} (1 - \kappa j \quad 1 - \kappa j \quad (1 - \kappa j)^{-1})$ , where  $n_0$  is the refractive index of the substrate.

The thickness of the bottom PML was varied in order to verify its impact on the convergence of the losses. The results obtained for different PML absorption are shown in Fig. 20.

From the graph it can be seen that PMLs work as expected i.e. they absorb all the field provided they are sufficiently thick. The larger the absorption, the smaller the necessary thickness. This good performance can be attributed to the fact that the PMLs and their adjacent layers are uniform layers in which the solution is purely analytical and so no numerical errors occur. Therefore it is not necessary to implement gradual PMLs as it would be in the case of numerical approximation.

We have also performed a convergence analysis as a function of the width of the super-cell  $L$  (i.e. the total width of the computational domain)

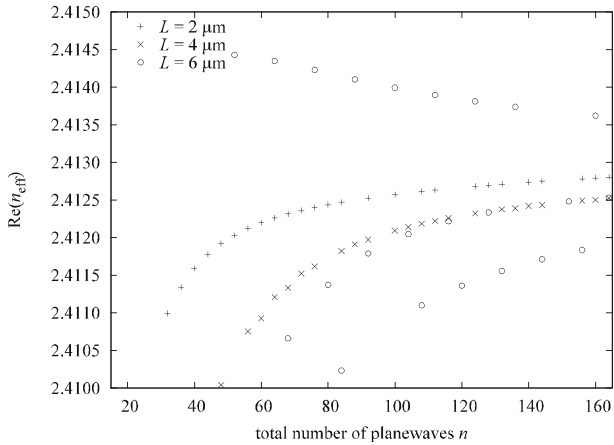


Fig. 21. The dependence of the real part of the effective index on the number  $n$  of plane-waves used for different super-cell sizes.

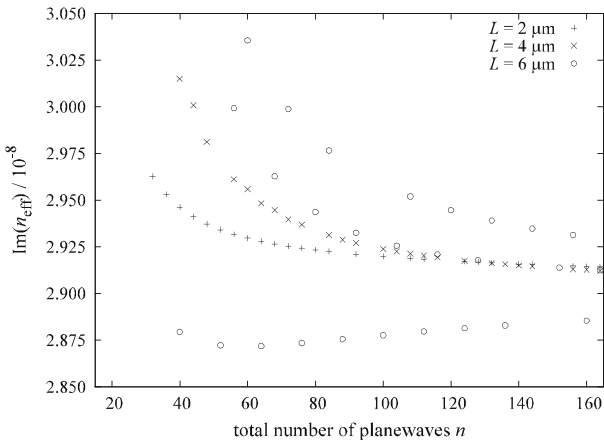


Fig. 22. The dependence of the imaginary part of the effective index on the number  $n$  of plane-waves used for different super-cell sizes.

and the number of plane waves  $n$  (corresponding to a total number of plane waves  $N = 2n + 1$ ). The results are presented in Figs. 21 and 22.

For larger super-cell sizes numerical artifacts appear in the form of oscillations. A closer look at Fig. 21 and 22 for  $L = 6 \mu\text{m}$  reveals that the results sub-converge to several different solutions, one of which is virtually the same as the stable one for  $L = 4 \mu\text{m}$ . Thus the chosen size of the super-cell should be small enough to avoid these oscillations, while on the other hand the super-cell should be large enough to give the field sufficient space to decay. The typical convergence time for the total number of plane waves

equal to  $n = 127$  ( $n = 255$ ) is 28 s (9 min respectively) on a 2.4 GHz PC, with the condition the good approximate initial guess is provided.

Analysing our results we have estimated the optimal value to be  $L = 4 \mu\text{m}$ . The best result obtained for this super-cell size is  $n_{\text{eff}} = 2.4126 - 2.910 \cdot 10^{-8} j$ .

### 12. Field profiles

In this section, we will focus on field plots obtained by several of the algorithms. In Fig. 23(b,f), we show transverse cuts defined in Fig. 23a for the modal  $x$ - and  $y$ -components of the electric-field. The calculation has been

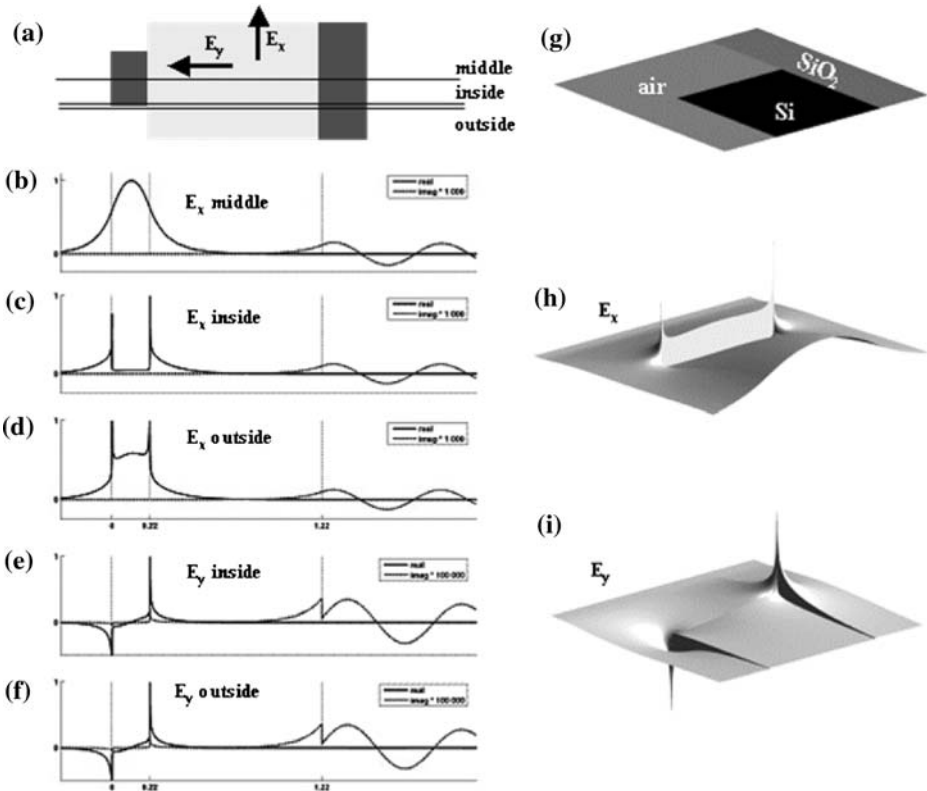


Fig. 23. Modal fields obtained with the aperiodic Fourier modal method. (a) Definition of the transverse cut at the middle of the waveguide and at corner edge. “Inside” and “outside” refer to transverse cuts in the ridge and out of the ridge, respectively. (b)–(d) :  $x$ -component of the electric field. (e)–(f) :  $y$ -component of the electric field. In (b)–(f), vertical dashed lines represent SiO<sub>2</sub>/Si interfaces. Note that the imaginary part in multiplied by 1000 in (b)–(d) and 100,000 in (e)–(f). (g) : half transverse section of the ridge. (h)–(i) : Corresponding real parts of  $E_x$  and  $E_y$ . Computational results are obtained for  $2M_x + 1 = 1001$ .

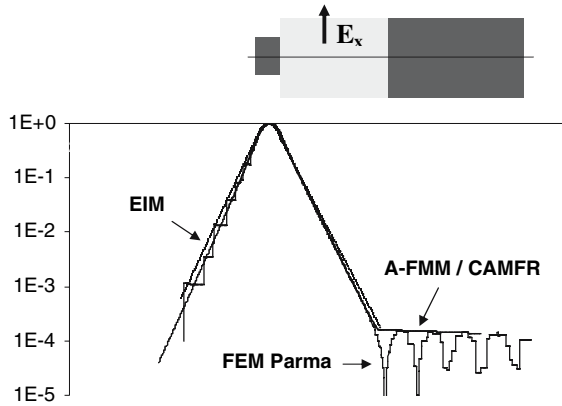


Fig. 24. The absolute value of  $E_x$  along the path shown in the inset for the effective index method, the FEM of Parma, the aperiodic fourier modal method and CAMFR.

performed by the aperiodic fourier modal method for 1001 retained Fourier harmonics. As shown, field discontinuities at the  $\text{SiO}_2/\text{Si}$  interfaces as well as field singularities at the corner are accurately described. This may appear surprising since one could expect that a method relying on Fourier expansions is not capable to calculate field discontinuities because of the inevitable Gibbs phenomenon. However, this possible source of artefact can be largely removed by considering Fourier expansions only for the fields which are continuous and then from their computation to derive the other discontinuous field components in real space directly from the constitutive relations. Details of the field computation technique used for these plots can be found in (Lalanne *et al.* 1998), along with an in-depth discussion of the computation accuracy at edge singularities by comparison with asymptotic closed-form expressions for the divergence at the corner. Finally note that the fields in Fig. 23(b–f) are obtained without smoothing the computational data neither in Fourier domain nor in real space.

If we were to make similar plots for other methods, they would be virtually indistinguishable on this scale. Therefore, we plot in Fig. 24 the absolute value  $|E_x|$  on a logarithmic scale for a few selected methods:

For the ‘exact’ methods, the difference between the curves in the neighbourhood of the core is hardly visible. The staircase profile for FEM Parma is because no interpolation was used within each finite element. The effective index method gives field profiles which are slightly larger than the exact methods. In the region of the substrate, the curves of the aperiodic fourier modal method and CAMFR are indistinguishable. FEM Parma shows some residual oscillations, which are probably due to parasitic reflections. (Note that the oscillations in Fig 23 should disappear in this plot, as we plot the absolute value).

Table 6. Summary of the results of all the methods

	$\text{Re}(n_{\text{eff}})$	$ \text{Im}(n_{\text{eff}})  \times 10^{-8}$
Effective index	2.45----	2.4----
Perturbation	2.35----	3.0----
BPM Obayya	2.413340	2.7----
FEM Uranus	2.4131..	2.97---
FEM Parma	2.41233_	2.45---
Olympios	2.413---	2.9----
FimmWave	2.41235_	2.688..
CAMFR	2.412372	2.9135_
Aperiodic fourier modal method	2.412372	2.91348
Plane wave admittance	2.4126..	2.910..

### 13. Summary

Table 6 summarises the results of all the methods.

As far as the approximate codes are concerned, it is interesting to point out that they give results which are more or less in the correct order of magnitude, with negligible numerical effort. Therefore, these tools still have their place as a first step in a design process.

When we look at the real part of index given by the other approaches, there is a general consensus that the first three significant digits are 2.41. For the digits after that, results vary between 2, 3 and 4. This spread is remarkable given that most of the methods claim much more significant digits. Within these codes, four agree on 5 significant digits 2.4123 (FEM Parma, FimmWave, CAMFR and aperiodic fourier modal method). The last two of these even agree up to 7 significant digits, although the convergence of the aperiodic fourier modal method is less oscillatory than that of the film mode matching. This is probably due to the ‘smoother’ nature of plane waves as compared to film modes.

The spread on the imaginary part, however, is significantly higher, with just barely an agreement on the first significant digit. The following approaches agree up to 2 significant digits 2.9: FEM Uranus, Olympios, CAMFR, aperiodic fourier modal method and plane wave admittance. The last three of these agree on 3 significant digits, and CAMFR and the aperiodic fourier modal method agree on 5 significant digits after rounding.

### 14. Conclusion

We presented simulation results on the complex effective index of a leaky photonic wire, using a wide variety of simulation tools. The convergence of those approaches was analysed and compared.

## Acknowledgements

This work has been performed in the framework of the European COST P11 action. Maciej Dems would like to acknowledge the support of Polish Ministry of Science and Higher Education in a grant number N202 025 31/0952. Philippe Lalanne and Jean Paul Hugonin acknowledge earlier discussions with Ignacio del Villar and Ignacio R. Matias and financial support from the WP1 of NEMO.

## References

- Andreani, L.C. and D. Gerace. *Phys. Rev. B* **73** 235114, 2006.
- ARPACK Software, available from <http://www.caam.rice.edu/pub/software/ARPACK>.
- Bienstman, P. *Opt. Quantum Electron.* **36** 5, 2004.
- CAMFR, available from <http://camfr.sourceforge.net>
- Conradi, O. S. F. Helfert and R. Pregla. *IEEE J. Quantum Electron.* **37**, 928, 2001.
- COST P11 website: <http://w3.uniroma1.it/energetical/>
- Ctyroky, J., S. Helfert, R. Pregla, P. Bienstman, R. Baets, R. De Ridder, R. Stoffer, G. Klaasse, J. Petracek, P. Lalanne, J.P. Hugonin, and R.M. De La Rue. *Opt. Quantum Electron.* **34** 455, 2002.
- Cucinotta, A, G. Pelosi, S. Selleri, L. Vincetti, and M. Zoboli. *Microwave Opt. Technol. Lett.* **23** 67, 1999.
- Czyszanowski, T., M. Dems, H. Thienpont, and K. Panajotov. *Proc. SPIE* **6185** 61850Y, 2006.
- Dems, M., R. Kotynski, and K. Panajotov. *Opt. Express* **13** 3196, 2005.
- Dems, M and K. Panajotov. 8th International Conference on Transparent Optical Networks, ICTON 2006, Nottingham UK, 18–22 Jun 2006.
- Dems, M., T. Czyszanowski. and K. Panajotov. *Proc. SPIE* **6182** 618219, 2006.
- Dumon, P., W. Bogaerts, J. Van Campenhout, V. Wiaux, J. Wouters, S. Beckx, D. Taillaert, B. Luyssaert, P. Bienstman, D. Van Thourhout and R. Baets. *IEEE Photonics Technol. Lett.* **16** 1328, 2004.
- Fimmwave, ver. 4.4 by Photon Design, <http://www.photond.com>
- Ghatak, A.K., K. Thyagarajan and M.R. Shenoy. *J. Lightwave Technol.* **5** 660, 1987.
- Hugonin, J.P., P. Lalanne, I. del Villar and I.R. Matias. *Opt. Quantum Electron.* **37** 107, 2005.
- Hugonin, J.P. and P. Lalanne. *J. Opt. Soc. Am. A* **22** 1844, 2005.
- Johnson, S.G., M. Ibanescu, M.A. Skorobogatiy, O. Weisberg, J.D. Joannopoulos and Y. Fink. *Phys. Rev. E* **65** 066611, 2002.
- Lalanne, P. and M. P. Jurek. *J. Mod. Opt.* **45** 1357, 1998.
- Li, L. *J. Opt. Soc. Am. A* **13** 1024, 1996.
- Moharam, M.G., E.B. Grann, D.A. Pommet and T.K. Gaylord. *J. Opt. Soc. Am. A* **12** 1068, 1995.
- Obayya, S.S.A., B.M.A. Rahman and H.A. El-Mikati. *J. Lightwave Technol.* **18** 409, 2000.
- Obayya, S.S.A., B.M.A. Rahman, K.T.V. Grattan and H.A El-Mikati. *J. Lightwave Technol.* **20** 1054, 2002.
- Olympios, <http://www.c2v.nl>
- Selleri, S. and J. Petracek. *Opt. Quantum Electron.* **33** 373, 2001.
- Selleri, S, L.A. Vincetti, A. Cucinotta and M. Zoboli. *Opt. Quantum Electron.* **33** 359, 2001.
- Silberstein, E., P. Lalanne, J.P. Hugonin and Q. Cao. *J. Opt. Soc. Am. A* **18** 2865 2001.
- Sudbo, A.S. *Pure Appl. Opt.* **2** 211, 1993.
- Tamir, T. *Guided-Wave Optoelectronics*, Chap. 2. Springer-Verlag.
- Tsuji, Y. and M. Koshiba. *J. Lightwave Technol.* **18**,618, 2000.

- Uranus, H.P., H.J.W.M. Hoekstra and E. van Groesen. *J. Nonlinear Opt. Phys. Mater.* **13** 175, 2004.
- Vassallo, C., *Opt. Quantum Electron.* **29** 95, 1997.
- Wijnands, F., H.W.M. Hoekstra, G.J.M. Krijnen and R.M. de Ridder. *J. Lightwave Technol.* **12** 2066, 1994.
- Xu, C.L., W.P. Huang and S.K. Chaudhuri. *J. Lightwave Technol.* **11** 1209, 1993.